Research Square

Preprints are preliminary reports that have not undergone peer review.
They should not be considered conclusive, used to inform clinical practice,
or referenced by the media as validated information.

Quantitative measurement of insulin-like growth factor-1 in saliva using multi-walled carbon nanotubes- based immunosensor

Ze Ren Chen
Universiti Malaya
Nor Syafirah Zambry
Universiti Malaya
Fatimah Ibrahim
fatimah@um.edu.my

Universiti Malaya
Norrima Mokhtar
Universiti Malaya
Wan Nurazreena Wan Hassan
Universiti Malaya
Wan Ahmad Hafiz Wan Md Adnan
Universiti Malaya
Bojan Petrović
University of Novi Sad
Sanja Kojić
University of Novi Sad
Goran M Stojanoić
University of Novi Sad

Research Article

Keywords:

Posted Date: August 3rd, 2026

DOI: https://doi.org/10.21203/rs.3.rs-9812101/v1

License: This work is licensed under a Creative Commons Attribution 4.0 International License.
Read Full License

Additional Declarations: No competing interests reported.

Quantitative measurement of insulin-like growth factor-1 in saliva using multi-walled carbon nanotubes-based immunosensor

Chen Ze Ren[1,2,3], Nor Syafirah Zambry[1,2] , Fatimah Ibrahim (corresponding author)[1,2*], Norrima Mokhtar[2,3,4], Wan Nurazreena Wan Hassan[2,5], Wan Ahmad Hafiz Wan Md Adnan[2,6], Bojan Petrović[7], Sanja Kojić[8], Goran M Stojanoić[8]

1 Department of Biomedical Engineering, Faculty of Engineering, Universiti Malaya, Kuala Lumpur, Malaysia.

2 Centre for Innovation in Medical Engineering (CIME), Universiti Malaya, Kuala Lumpur, Malaysia.

3 Department of Electrical Engineering, Faculty of Engineering, Universiti Malaya, Kuala Lumpur, Malaysia.

4 Malaysia-Japan Research Center, Universiti Malaya, Kuala Lumpur, Malaysia.

5 Department of Paediatric Dentistry and Orthodontics, Faculty of Dentistry, Universiti Malaya, Kuala Lumpur, Malaysia.

6 Department of Medicine, Faculty of Medicine, University Malaya Medical Centre, Kuala Lumpur, Malaysia.

7 Department of Dental Medicine, Faculty of Medicine, University of Novi Sad, Novi Sad, Serbia.

8 Faculty of Technical Science, University of Novi Sad, Novi Sad, Serbia.

*Corresponding author. E-mail address: fatimah@um.edu.my

ABSTRACT

Growth-related assessment commonly involves insulin-like growth factor-1 (IGF-1), which is used to monitor bone and skeletal maturity and to support orthodontic treatment planning. Compared with conventional blood-based assays, saliva is a painless and easily accessible biological matrix that allows repeated assessment of IGF-1. Existing approaches for salivary IGF-1 analysis predominantly depend on centralized laboratory techniques such as enzyme-linked immunosorbent assay (ELISA), radioimmunoassay (RIA), and mass spectrometry (MS), which are time-consuming, operationally complex, and high-cost procedures. This study presents a rapid and straightforward multi-walled carbon nanotubes (MWCNTs)-based immunosensor for the quantitative measurement of IGF-1 in saliva. A label-free electrochemical immunosensor was constructed on a MWCNTs screen-printed carbon electrode (MWCNTs-SPCE). The modified MWCNTs-SPCE was immobilized with anti-IGF-1 monoclonal antibodies to detect the presence of IGF-1 in saliva. The stepwise fabrication process of the label-free electrochemical immunosensor was characterized morphologically and structurally by scanning electron microscopy (SEM), Fourier-transform infrared spectroscopy (FTIR), X-ray diffraction (XRD), and Raman spectroscopy. Electrochemical characterization of the MWCNTs-SPCE was carried out using cyclic voltammetry (CV) and differential pulse voltammetry (DPV). Under optimized conditions, the immunosensor displayed a linear response to IGF-1 from 1 to 100 μg/mL in 0.01 M phosphate-buffered saline (R^2 = 0.998), achieving a limit of detection(LOD) of 0.95 μg/mL and a limit of quantification(LOQ) of 3.19 μg/mL within 30 min. Importantly, the study also demonstrates that the immunosensor successfully detects a range of IGF-1 concentrations from 1 to 100 μg/mL in synthetic saliva with a LOD of 0.99 μg/mL and LOQ of 3.3 μg/mL, highlighting its sensitivity and analytical reliability in practical clinical settings.

1. Introduction

As a primary mediator of growth hormone (GH), IGF-1 reaches its peak production during the adolescent growth spurt, where it is pivotal for teenage growth and development [1], [2], [3], [4]. It not only influences muscle development and cell proliferation but also stimulates skeletal growth, making it a valuable consideration in orthodontic treatment planning. Numerous findings indicate a significant correlation between IGF-1 and skeletal maturity [3], [5]. Therefore, continuous monitoring of IGF-1 concentration in the body provides essential information about growth maturity and bone remodeling patterns. However, assessing IGF-1 levels for patient monitoring using conventional biofluids, such as blood, entails invasive methods, requires trained personnel, and necessitates complex laboratory infrastructure, significantly increasing both the time and cost of testing and analysis. These limitations have led researchers to explore alternative sample matrices that are easier and less burdensome to collect. Saliva is increasingly recognized as a non-invasive biological fluid for biomarker assessment, as it can be collected painlessly and repeatedly without specialized skills, thereby improving patient compliance and enabling longitudinal monitoring. Recent studies have highlighted the advancing status of saliva-based diagnostics and their potential role as a practical alternative to blood-based assays in various clinical contexts [6], [7].

Additionally, extensive clinical evidence supports the significance of salivary IGF-1 as a valuable biomarker. Previous studies have shown that hormones and growth factors, including IGF-1, are present in saliva in forms similar to those found in blood. The levels of these substances in saliva reflect their concentrations in the bloodstream, as reported by Balashova [8]. Moreover, changes in salivary IGF-1 levels have been linked to specific pathological conditions. For instance, Paszynska reported significantly reduced IGF-1 levels in patients with anorexia nervosa [9]. These findings highlight the clinical significance of salivary IGF-1 and reinforce its potential as a non-invasive biomarker for physiological and pathological monitoring. However, the concentration of IGF-1 in saliva can be influenced by several factors, including physiological variations such as age and hormonal status[10], as well as matrix-related interferences, including protein adsorption, enzymatic degradation, and dilution effects. These factors may impact the accuracy and reliability of electrochemical detection[11].

Clinical studies have found that the concentration of IGF-1 in human saliva is typically in the low nanogram per milliliter (ng/mL) range and varies significantly with skeletal maturity stages. For instance, salivary IGF-1 levels have been reported to be approximately 0.93 ng/mL at the prepubertal stage, increasing to around 2.52–2.58 ng/mL during peak pubertal development, followed by a decline to 1.09–1.67 ng/mL as growth decelerates toward completion. These variations demonstrate a strong correlation between salivary IGF-1 levels and growth maturity, with statistically significant differences observed across developmental stages and a positive correlation coefficient ($r \approx 0.6$) [12].

Additionally, salivary IGF-1 and IGFBP-3 levels correlate with systemic changes associated with bone development, supporting saliva as a non-invasive medium for monitoring growth biomarkers[13]. The simplicity and painless nature of saliva collection make it ideal for frequent monitoring, particularly for pediatric patients, point-of-care screening, and longitudinal studies [14]. Furthermore, studies have found significant correlations between specific salivary biomarkers and their serum counterparts, enhancing saliva's diagnostic potential [15], [16]. However, key analytes like IGF-1 are present in much lower concentrations in saliva than in serum, making them susceptible to dilution, enzymatic degradation, and interference from components like mucins, posing challenges for reliable detection [17].

Several analytical approaches have been reported for detecting IGF-1 biomarkers in saliva. Conventional immunoassay techniques are commonly employed for IGF-1 monitoring because of their high specificity and sensitivity, with enzyme-linked immunosorbent assays (ELISA) and chemiluminescent immunoassays (CLIA) being representative approaches. Nevertheless, these techniques are labor-intensive, time-consuming, and require complex processing steps, which limit their application for rapid or real-time monitoring. Radioimmunoassay (RIA) has also been utilized for IGF-1 monitoring; however, it involves radioactive reagents and associated safety and logistical constraints. Liquid chromatography–tandem mass spectrometry (LC–MS/MS) offers excellent specificity and multiplexing capabilities. It has become increasingly used in salivary biomarker research, but it requires complex sample preparation, expensive instrumentation, and centralized lab infrastructure [18], [19]. Although existing studies have demonstrated that saliva is an ideal non-invasive medium for monitoring growth-related biomarkers, their limitations highlight the need for alternative detection methods that are rapid, cost-effective, simple, user-friendly, portable, and practical for point-of-care applications.

To address the increasing demand for a higher-sensitivity, rapid, and portable detection method for monitoring IGF-1 in saliva, researchers are focusing on nano-based electrochemical biosensor platforms. These platforms show great potential for rapid, simple, and highly sensitive IGF-1 detection in saliva. Several studies have reported the development of biosensors for detecting IGF-1 in blood or buffer matrices, achieving good sensitivity and detection limits. For instance, a nanofiber/reduced graphene oxide-based immunosensor has reached a detection limit as low as 55.72 fg/mL in plasma samples, while a carbon nanotube-based immunosensor has enabled picogram-level detection of IGF-1 in serum [20], [21]. Despite promising detection performance, many reported biosensor systems require further validation through clinical studies and specific optimization for detecting low concentrations of IGF-1[22]. Moreover, their performance has not yet been validated in saliva, a complex biological matrix characterized by low analyte concentrations and substantial interference. Notably, to date, no electrochemical biosensor has been reported for the direct detection of IGF-1 in saliva.

Therefore, this study aims to develop a simple, rapid, sensitive, and non-invasive platform for precise quantification of salivary IGF-1. This approach overcomes the limitations of the current electrochemical platform for detecting salivary IGF-1, making it ideal for point-of-care (POC) clinical testing and continuous monitoring applications. In sensor design, selecting a suitable electrode substrate is crucial for achieving optimal detection performance. SPCEs offer advantages such as low cost, disposability, mass manufacturability, and ease of integration into point-of-care devices, and they have been widely used for salivary biomarker detection, including lactate, glucose, and interleukin-6 [23], [24]. To date, many studies have incorporated nanomaterials, including graphene oxide (GO), reduced graphene oxide (rGO), and MWCNTs on the electrochemical sensing platform to address the analytical challenges posed by low-abundance targets such as salivary IGF-1. These materials contribute to an enlarged effective surface area and enhanced electron transfer, thereby providing a stable platform for antibody immobilization [25], [26].

This study introduces the development of a label-free, highly sensitive electrochemical immunosensor utilizing an MWCNTs-SPCE platform for quantifying IGF-1 in saliva. To the best of our knowledge, this study is the first validated electrochemical biosensor specifically designed for the detection of salivary IGF-1. The developed immunosensor offers straightforward operation and rapid detection time, showing great potential for POC testing and clinical applications in assessing salivary IGF-1 levels. Anti-IGF-1 antibodies were introduced to the MWCNTs-SPCE to confer molecular recognition capability toward the target antigen. The successful fabrication of the immunosensor was

confirmed by cyclic voltammetry (CV) and differential pulse voltammetry (DPV). The proposed immunosensor exhibited reliable analytical performance toward IGF-1 over a broad concentration range when evaluated in an artificial saliva matrix. Owing to its straightforward detection strategy, this electrochemical platform shows considerable promise for the clinical determination of salivary IGF-1. The proposed platform demonstrates several practical advantages that distinguish it from conventional IGF-1 detection methods. It enables rapid analysis within approximately 30 minutes using a minimal sample volume of 10 μL, significantly reducing both assay time and sample consumption compared to standard laboratory-based techniques. More critically, this study represents the first reported electrochemical immunosensor for the direct detection of IGF-1 in saliva, addressing a key limitation in current biosensing strategies that are predominantly restricted to serum or buffer systems. By integrating a non-invasive sampling approach with a simplified and scalable electrochemical platform, this work advances the development of POC diagnostics and provides a promising pathway toward real-time, longitudinal monitoring of growth-related biomarkers in clinical and orthodontic applications.

2. Materials and methods

2. 1 Materials

The anti-IGF-1 antibody (rabbit polyclonal; FNab09936) and IGF-1 antigen (recombinant human; P2663) were purchased from FineTest Biotech Co., Ltd. (China). Artificial saliva was obtained from Beijing Sola Biotechnology Co., Ltd. (China). The chemical reagents used in this study comprised 1-ethyl-3-(3-dimethylaminopropyl) carbodiimide hydrochloride (EDC), N-hydroxysuccinimide (NHS), and an aqueous graphene oxide (GO) dispersion (2 mg/mL), all sourced from Sigma-Aldrich (USA). The buffer solutions and chemical reagents used in this study were supplied by Thermo Fisher Scientific Inc. (USA), including phosphate-buffered saline (10× PBS, pH 7.4), potassium ferricyanide ($K_3Fe(CN)_6$), potassium ferrocyanide trihydrate ($K_4Fe(CN)_6 \cdot 3H_2O$), 0.1 M BupHTM-MES buffer saline (pH 4.7), and sodium dodecyl sulfate (SDS, 99%). Standard-grade bovine serum albumin (BSA) with a pH of 7.0 was sourced from Capricorn Scientific GmbH (Germany). Carboxyl-modified MWCNTs with a purity exceeding 96% were sourced from Nanografi Nanotechnology Co. (Türkiye). The nanotubes exhibited outer diameters of 8–18 nm and lengths ranging from 10 to 35 μm. Screen-printed carbon electrodes (SPCEs, DRP-110) and the potentiostat (μStat-i 400s) were procured from Metrohm AG (Switzerland). Throughout this study, deionized (DI) water (18.2 MΩ·cm at 25 °C, Milli-Q® system) was used to prepare all aqueous solutions, and all other chemicals were of analytical grade.

2. 2 Preparation of Multiple Nanomaterial Screen-Printed Electrode

Carboxyl-functionalized multi-walled carbon nanotube (MWCNTs–COOH) powder was probe-sonicated for 30 min in deionized water containing 2% (w/v) sodium dodecyl sulfate (SDS) to obtain a homogeneous suspension, which was adjusted to a final SDS concentration of 0.25% (w/v) and directly used for electrode modification. GO was dispersed in DI water and sonicated for 2 h to form a homogeneous suspension (1% w/v), after which the resulting dispersion was used to modify the working electrode surface, yielding GO-SPCE.

Reduced graphene oxide (rGO) was prepared via electrochemical reduction of the GO-SPCE. Briefly,

The GO-SPCE was drop with 0.5 M H_2SO_4 aqueous solution and subjected to CV scans at a scan rate of 0.1 V s^{-1} over the potential range of 0 to 1.6 V, with three consecutive scan cycles performed. After electrochemical reduction, the rGO-modified electrode was thoroughly rinsed with DI water and dried at room temperature.

Unless otherwise stated, nanomaterial-modified electrodes were fabricated by depositing 2.5 μL of the respective dispersions onto the working electrode, which were then allowed to dry under ambient conditions for approximately (28 ± 2 °C).

2. 3 Assembly of the electrochemical immunosensor for IGF-1 analysis

Fig. 1. depicts the fabrication process of the electrochemical immunosensor, together with a schematic showing the anticipated interactions between anti-IGF-1 antibodies and the three-dimensional MWCNT network. First, the surface carboxyl moieties on the MWCNTs-SPCE were activated by adding 10 μL of an EDC/NHS mixture (0.1 M EDC and 0.025 M NHS) and incubating for 45 minutes. The electrode was gently rinsed with 0.1M PBS buffer to ensure complete removal of unreacted reagents and to avoid non-specific crosslinking before antibody immobilization. After that, 10 μL of a monoclonal IGF-1 antibody (4 μg/mL in 0.1 M PBS) was applied and incubated for one hour at 28 ± 2 °C for covalent immobilization. Unbound antibodies were removed by gentle washing. Subsequently, nonspecific sites were blocked with 5 μL of 1% (w/v) BSA for one hour, then rinsed and dried. Finally, antigen-antibody recognition was performed by introducing 10 μL of IGF-1 antigen solution (100 μg/mL). Conducted at room temperature (28 ± 2 °C), all electrochemical measurements employed a 0.01 M $[Fe(CN)_6]^{3-/4-}$ solution using 0.1 M KCl as the supporting electrolyte.

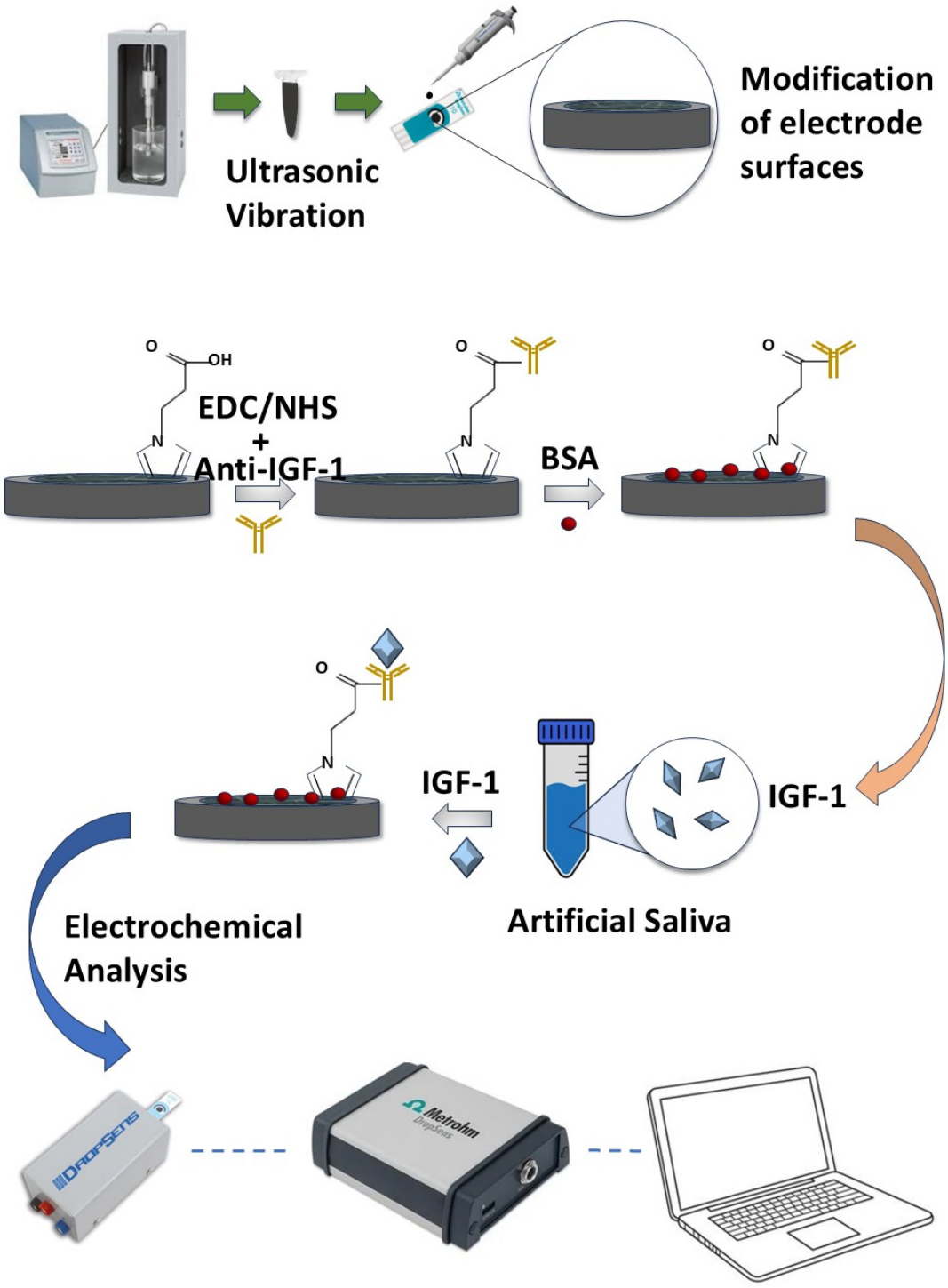


Fig. 1 Schematic diagram of the preparation process for label-free immunosensors for IGF-1 detection.

2. 4 Morphological characterization

To characterize the modified electrodes, structural and chemical analyses were performed. Surface features of the modified electrodes were examined by FESEM–EDX at the Institute of Advanced Studies(IAS), Universiti Malaya, using a Quanta 450 FEG system (FEI). Imaging was carried out at multiple magnifications (10k, 50k, and 100k) across four quadrants of the working electrode.

Concurrently, the chemical functional groups were identified using FTIR spectroscopy (PerkinElmer Spectrum 400) at the Chemistry Department Central Facility of the same university. XRD analysis was performed at the Low Dimensional Materials Research Centre, Universiti Malaya, using a Rigaku diffractometer to investigate the crystalline structure of the materials. Raman spectroscopy measurements were carried out at the Physics Department, Faculty of Science, Universiti Malaya, to characterize the surface properties of SPCEs modified with different concentrations of MWCNTs.

2. 5 Electrochemical measurements

A portable dual channel potentiostat (μStat 40, DropSens, Spain) interfaced to the DropView 8400 software was employed to perform all electrochemical measurements. The stepwise fabrication of the sensor was characterized by CV, scanning from −0.2 to +0.8 V at 0.1 V s^{-1}. In this study, compared to CV, DPV exhibits superior sensitivity in capturing subtle signal changes [27], [28]. Therefore, DPV was used for the quantitative detection of IGF-1. The optimized DPV parameters were: potential range, −0.1 to +0.4 V; pulse amplitude, 0.05 V; pulse width, 20 ms; step potential, 0.004 V; and a scan rate of 0.01 V s^{-1}. All measurements were performed at 28 ± 2 °C in a solution of 0.01 M $[Fe(CN)_6]^{3-/4-}$ and 0.1 M KCl. Reproducibility was evaluated through triplicate measurements (n = 3) using independently prepared electrodes. Data were processed in OriginPro 2024 to calculate the mean ± standard deviation (SD). Statistical analysis was performed in GraphPad Prism 8.0.2 using one-way ANOVA with Tukey's post hoc test, with $p < 0.05$ was considered significant.

3. Results and discussion

3. 1 Electrochemical performance of different nanomaterials

In this study, several nanomaterials, including GO, rGO, and MWCNTs, at a concentration of 1%(w/v) were evaluated to determine the optimal working electrode material for the development of an immunosensor. The electrochemical performance (CV and DPV) of the different nanomaterials is demonstrated in Fig. 2.

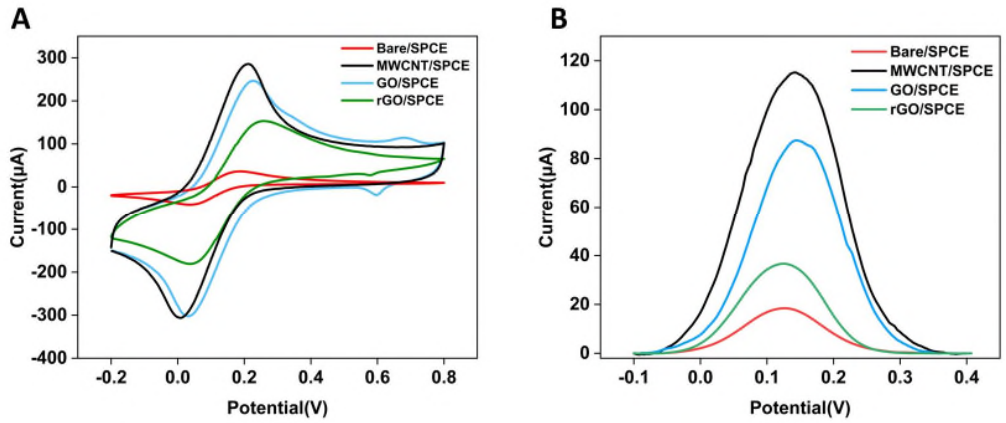


Fig. 2 Electrochemical characterization of SPCE modified with different nanomaterials. (A) Cyclic voltammetry (CV) responses of bare SPCE, GO-SPCE, rGO-SPCE, and 1 %(w/v) MWCNT/SPCE

recorded in the redox probe solution, showing the effect of nanomaterial modification on electron transfer behavior. (B) Differential pulse voltammetry (DPV) responses of bare SPCE, GO-SPCE, rGO-SPCE, and 1% (w/v) MWCNTs-SPCE, revealing a substantially increased peak current following MWCNT modification and suggesting improved electrochemical activity compared with GO- and rGO-modified electrodes.

Fig. 2 illustrates the electrochemical performance of SPCEs modified with MWCNTs, GO, and rGO. In cyclic voltammetry, the MWCNTs/SPCE exhibited the highest anodic and cathodic peak currents, indicating superior electrochemical activity. Specifically, the anodic peak current (I_{pa}) of the MWCNTs/SPCE reached 285.21 μA, which was significantly higher than those of the GO/SPCE (245.92 μA) and rGO/SPCE (153.02 μA). Similarly, the corresponding cathodic peak current (| I_{pc} |) of the MWCNTs/SPCE was 306.13 μA, exceeding that of the GO/SPCE (302.13 μA) and markedly higher than that of the rGO/SPCE (180.63 μA). These results demonstrate a pronounced enhancement in electron-transfer efficiency induced by MWCNT modification. Consistent with the CV results, differential pulse voltammetry further confirmed the superior performance of the MWCNT-modified electrode. The DPV peak current (I_p) obtained at the MWCNTs/SPCE (115.14 μA) was substantially higher than those recorded for the GO/SPCE (87.48 μA) and rGO/SPCE (36.58 μA), indicating an increased electroactive surface area and enhanced electron-transfer kinetics. These enhancements are attributed to the unique characteristics of carbon nanotubes, including their high aspect ratio, good conductivity, and efficient charge transfer capabilities [29], [30]. Such improvements are crucial for achieving measurable signal modulation upon biomolecule binding, especially for the recognition of low-abundance targets like IGF-1 in complex matrices such as saliva [31]. Accordingly, MWCNTs were selected as the optimal nanomaterial for developing the immunosensor in the next experiment.

3. 2 Morphological characterization of MWCNTs/SPCE

The spatial arrangement of MWCNTs across the SPCE working electrode was examined using FESEM (Fig. 3). At 0.25%(w/v) concentration (Fig. 3A-C), the MWCNTs are sparsely dispersed with significant substrate exposure (Fig. 3A). Individual tubes appear as well-separated fibers with relatively aligned orientations and minimal intertwining (Fig. 3B), which favors the formation of direct electron-conduction paths. At a higher magnification (Fig. 3C), the tubular structure is distinctly visible, confirming that the low concentration facilitates the discrete arrangement of individual MWCNTs. In contrast, at a 1% (w/v) concentration (Fig. 3D-F), the surface is covered by a densely packed, continuous MWCNT film with almost no bare substrate visible (Fig. 3D). The carbon tubes are densely interlaced and entangled, forming a complex three-dimensional network (Fig. 3E). However, as shown in the high-magnification image (Fig. 3F), localized agglomeration occurs where the tubes are entangled into clusters. This inhomogeneous packing can increase contact resistance and impede electron transport, potentially reducing the conductivity of the composite. Overall, FESEM results indicate that as the MWCNTs concentration increases from 0.25% (w/v) to 1% (w/v), the electrode surface morphology evolves from a relatively dispersed nanotube structure to a dense, continuous network structure. However, excessively high loading simultaneously introduces significant local agglomeration, which may compromise interfacial uniformity and adversely affect subsequent functionalization and biomolecular immobilization. In contrast, electrodes modified with low concentrations of MWCNTs exhibited a more uniform and controllable surface structure.

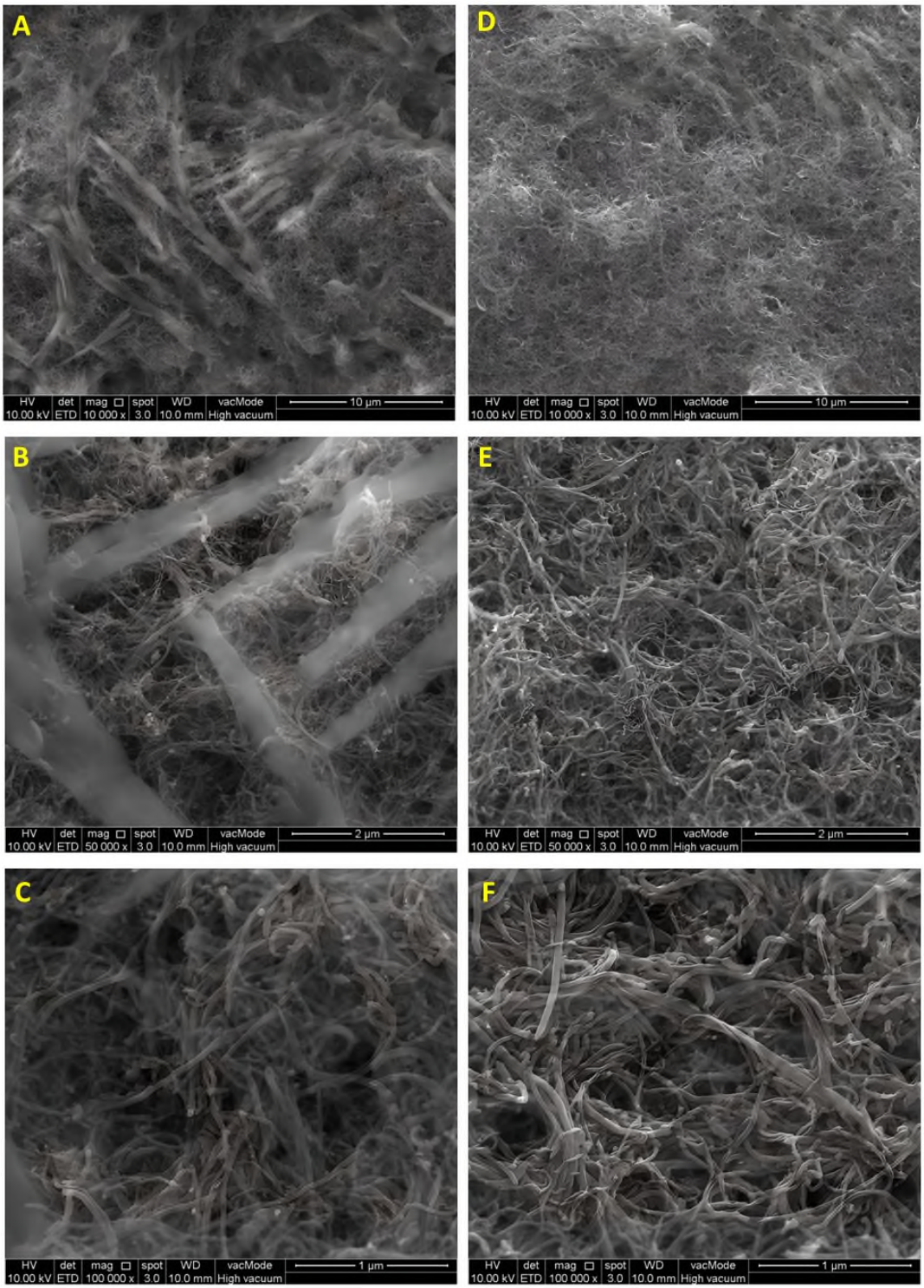
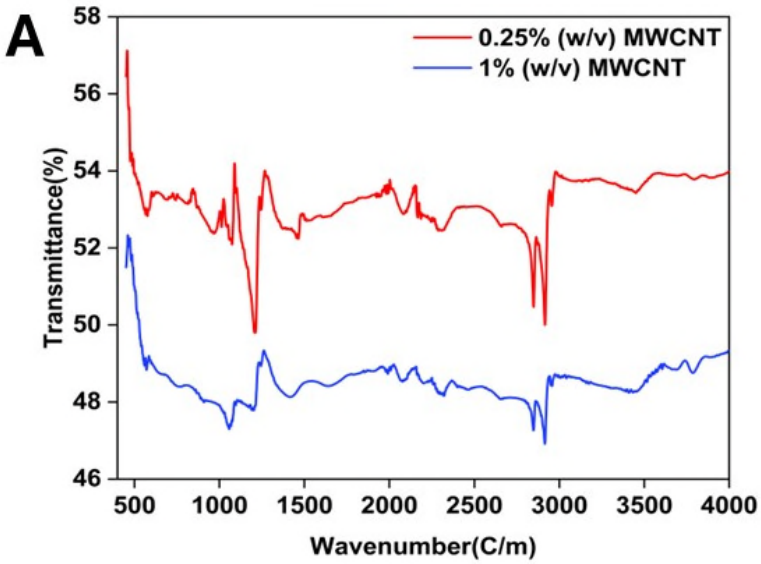
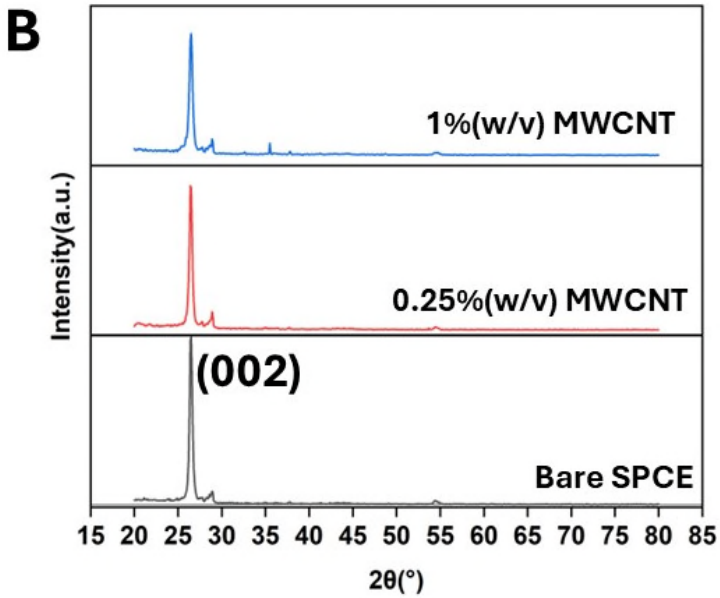


Fig. 3 (A–C) SPCE modified with 0.25 % (w/v) MWCNTs recorded at magnifications of 10k, 50k, and 100k, respectively; (D–F) SPCE modified with 1 % (w/v) MWCNTs recorded at magnifications of 10k, 50k, and 100k, respectively.

The physicochemical properties of SPCE modified with MWCNTs at concentrations of 0.25% (w/v) and 1%(w/v) were further characterized using FTIR, XRD, and Raman spectroscopy (Fig. 4). The FTIR spectrum of the 0.25% (w/v) MWCNTs sample (Fig. 4 A) indicates a prominent band in the 1410–1388 cm^{-1} region, characteristic of the O–H bending vibration from surface carboxyl (–COOH) groups. In

contrast, the intensity of this absorption band is noticeably reduced in the 1% (w/v) MWCNTs sample. In addition, a C–O stretching vibration band is observed at 1283–1235 cm^{-1} for the 0.25% (w/v) MWCNTs sample, whereas multiple absorption peaks appear at 1261, 1232, and 1209 cm^{-1} in the 1% (w/v) MWCNTs spectrum, demonstrating concentration-dependent changes in surface chemical functionalities [32], [33]. Therefore, FTIR results show that lower MWCNTs concentrations are more conducive to preserving accessible carboxyl (–COOH) functional groups, thereby providing a more favorable surface chemical environment for the efficient and stable immobilization of subsequent biological receptors.


A
0.25% (w/v) MWCNT
1% (w/v) MWCNT
Transmittance(%)
58
56
54
52
50
48
46
500
1000
1500
2000
2500
3000
3500
4000
Wavenumber(C/m)


B
1%(w/v) MWCNT
0.25%(w/v) MWCNT
(002)
Bare SPCE
Intensity(a.u.)
15 20 25 30 35 40 45 50 55 60 65 70 75 80 85
2θ(°)

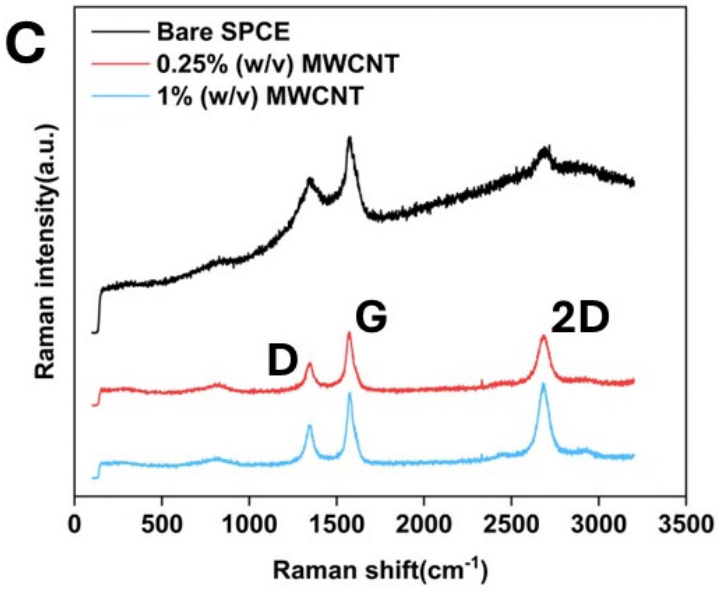

C
Bare SPCE
0.25% (w/v) MWCNT
1% (w/v) MWCNT
Raman intensity(a.u.)
D
G
2D
0
500
1000
1500
2000
2500
3000
3500
Raman shift(cm-1)

Fig. 4 Physicochemical characterization of SPCEs modified with different MWCNT concentrations. (A) FTIR spectra of 0.25 %(w/v) and 1 %(w/v) MWCNTs, showing concentration-dependent surface functional groups; (B) XRD patterns of bare SPCE and SPCE modified with 0.25 %(w/v) and 1 %(w/v) MWCNTs, highlighting the graphitic (002) diffraction peak at $2\theta \approx 26.4°$;(C) Raman spectra of bare and MWCNTs-SPCE, displaying the characteristic D, G, and 2D bands and illustrating the effect of MWCNT concentration on nanotube loading and structural order.

The XRD patterns shown in Fig. 4B demonstrates that all samples exhibit a characteristic diffraction peak at $2\theta \approx 26.4°$, corresponding to the (002) plane of graphitic carbon. Compared with the bare SPCE, the diffraction intensity decreases after modification with MWCNTs. Among the modified electrodes, the SPCE coated with 0.25% (w/v) MWCNT displays a higher (002) peak intensity than that coated with 1% (w/v) MWCNTs. This result indicates that as the MWCNTs concentration increases, the nanotubes become more prone to aggregation and exhibit random orientation, thereby obscuring the underlying graphite structure to some extent and leading to a reduction in the intensity of the characteristic (002) diffraction peak.

The presence of MWCNTs on the electrode surface was confirmed by Raman spectroscopy (Fig. 4C), which showed distinct D, G, and 2D bands at approximately 1341, 1572, and 2679 cm^{-1}, respectively. The intensities of these characteristic peaks increase with increasing MWCNTs concentration. The I_{D_band}/I_{G_band} ratio is approximately 0.58 for the 0.25% (w/v) MWCNTs-modified working electrode, whereas it increases to about 0.62 for the 1% (w/v) MWCNTs-modified working electrode, indicating a higher defect density at higher MWCNTs loading[34]. Raman results further indicate that while increasing the MWCNTs loading enhances surface coverage, it simultaneously introduces greater structural defects. This increased defect density may adversely affect the continuity of electron transport and the stability of interfaces.

These findings suggest that excessive MWCNTs loading does not necessarily improve electrode performance. SPCEs modified with 0.25% (w/v) MWCNTs achieve an optimal combination of uniform nanotube dispersion, surface functional group availability, and structural order. This optimized interface is expected to facilitate efficient electron transfer and ensure stable antibody immobilization, thus providing a robust sensing material for the constructing a high-performance electrochemical immunosensor for detecting salivary IGF-1.

3.3 Electrochemical behaviour of MWCNTs-SPCE

The DPV response of the working electrode at different MWCNTs concentrations (0.01%, 0.25%, 0.50%, 0.75%, and 1% (w/v)) are displayed in Fig. 5. It was shown that the working electrode modified with 0.25% (w/v) MWCNTs exhibited the highest peak current response, indicating optimal electron transfer activity under these conditions. This result suggests that at lower MWCNTs concentrations, the nanotubes are more uniformly dispersed on the electrode surface, providing abundant electroactive sites without significant aggregation that could impede electron mobility consistent with the morphological characterization results (Fig. 5A-C). A decrease in current response was observed as the MWCNTs concentration exceeded 0.50% (w/v). This decrease is attributed to nanomaterial agglomeration, which creates barriers to electron transport, diminishes the effective surface area, and reduces the accessibility

of active sites. Such agglomeration can also lead to non-uniform antibody immobilization, negatively affecting sensor reproducibility and sensitivity [35], [36]. The observed trend is consistent with literature reports where high nanomaterial loadings do not necessarily enhance sensor performance and may instead introduce mass transport limitations in electrochemical immunosensors [37]. Accordingly, 0.25% (w/v) was determined as the optimal MWCNTs concentration and was employed in all subsequent immunosensor preparations. This optimized MWCNTs-SPCE provides a stable and sensitive platform for further optimization of antibody concentration, antigen incubation conditions, and ultimately reliable detection of salivary IGF-1.

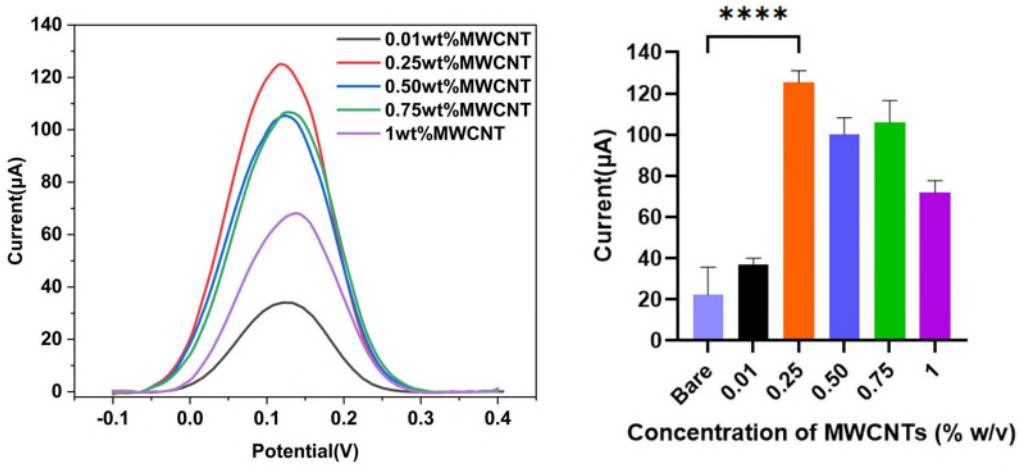


Fig. 5 Effect of MWCNTs concentration on the electrochemical response of SPCE. (A) Differential pulse voltammetry (DPV) curves of SPCE modified by MWCNTs. The peak current varies systematically with MWCNT concentration (0.01, 0.25, 0.50, 0.75, and 1% w/v). (B) Corresponding statistical analysis of DPV peak currents, showing that the 0.25 %(w/v) MWCNT-modified SPCE exhibits the highest current response. Data are presented as mean ± SD (n = 3). Asterisks denote statistical significance (****, $p < 0.0001$).

3. 4 Electrochemical Kinetics and Active Surface Area Determination

To investigate the electrochemical behavior of the MWCNTs-SPCE-modified electrode, cyclic voltammograms were recorded at different scan rates (10–500 mV/s) in a 5 mM $[Fe(CN)_6]^{3-/4-}$ solution (Fig. 6). As the scan rate increased, the peak current of the redox peak increased significantly, and the peak potential shifted slightly. Generally, if the peak current is linearly related to the scan rate itself, the electrode process is adsorption-controlled; if it is linearly related to the square root of the scan rate, it is diffusion-controlled. As can be seen from Fig. 7, the currents of both the anodic and cathodic peaks exhibit a good linear fit with $\nu^{1/2}$ (R^2 = [0.9878]), which clearly indicates that mass transfer in this system is diffusion-dominated.

On this basis, the electrochemical active surface area of the electrode was calculated using the Randles–Sevcik equation [20]:

$$I_p = 2.69 \times 10^5 \times A \times D^{1/2} \times n^{3/2} \times C \times \nu^{1/2}$$

Here, I_p (A) is the peak current, A is the effective area (cm^2), D is the diffusion coefficient at 25 °C

($[Fe(CN)_6]^{3-/4-}$ takes $[7.6\times10^{-6}]$ cm^2/s), n is the number of electron transfers (n = 1), and C is the probe concentration ($[5 \times 10^{-6}]$ mol/cm^3), and ν is the scan rate (V/s). Based on the slope (k = 0.0009148 $A\cdot s^{1/2}.V^{-1/2}$) of the linear fit of I_p versus $\nu^{1/2}$, the effective surface area of the MWCNTs-SPCE-modified electrode was calculated to be 0.2467 cm^2.

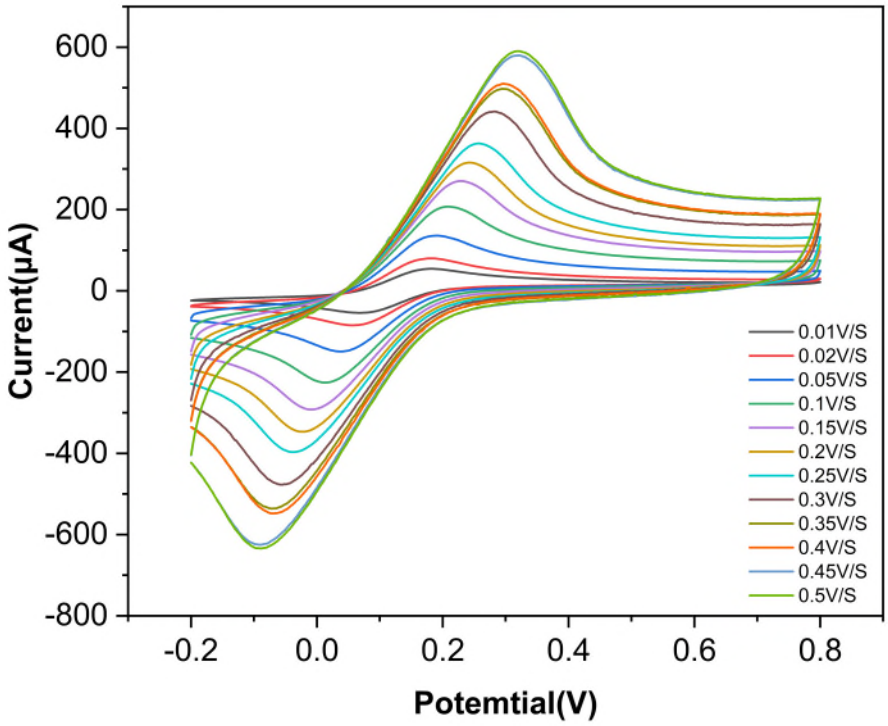


Fig. 6 shows the CVs of the MWCNT-modified electrode in 5 mM $[Fe(CN)_6]^{3-/4-}$solution at different scan rates (0.01–0.5 V/s). As the scan rate increases, both anodic and cathodic peak currents increase significantly, while the peak potentials exhibit slight shifts, indicating a typical quasi-reversible electrochemical behavior.

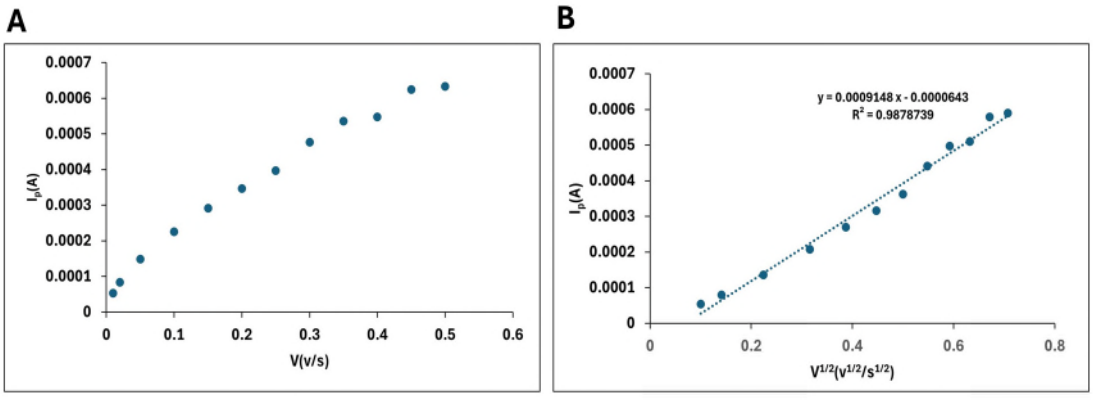


Fig. 7 A presents the relationship between peak current (Ip) and scan rate (ν), showing a nonlinear trend. In contrast, B demonstrates a good linear relationship between peak current and the square root of scan rate ($\nu^{1/2}$) with a high correlation coefficient ($R^2 \approx 0.99$), suggesting that the electrochemical process is predominantly diffusion-controlled

3. 5 Optimization studies

Optimization of the immunosensor focused on three experimental variables, namely antibody incubation time, antibody concentration, and antigen incubation time (Fig. 8). Antibody immobilization led to a marked change in the electrochemical signal, indicating effective antibody attachment onto the nanomaterial-modified electrode surface Fig. 8(a). Experimental results identified an incubation time of 15 min as the optimal condition. Compared with the bare MWCNT-modified electrode, a significant increase in current response was observed after 15 min of antibody incubation ($P < 0.0001$). Notably, no statistically significant difference in current response was detected between 15 min and longer incubation times (30–90 min) ($P > 0.05$), indicating that antibody adsorption rapidly reached a saturation plateau within 15 min.

Fig. 8(b) illustrates the differential pulse voltammetry (DPV) responses of the working electrode under varying antibody concentrations. The antibody-modified electrode exhibited distinctly different electrochemical behavior compared with the underlying MWCNT layer, highlighting the impact of surface functionalization. Optimization of antibody concentration indicated that 1 μg/mL produced the highest current response. Further increases to 4 or 10 μg/mL did not yield a statistically significant improvement in signal intensity ($P > 0.05$, ns; Tukey's multiple comparisons test), implying that the available immobilization capacity of the electrode surface was already fully utilized. Accordingly, 1 μg/mL was selected as the optimal antibody immobilization concentration and employed in all subsequent experiments.

Finally, the effect of antigen incubation time was evaluated, as shown in Fig. 8(c). The results indicate that 30 min is the optimal incubation period for the formation of stable antibody–antigen immunocomplexes. Prolonging the incubation time beyond 30 min did not further improve the sensing performance; instead, a slight increase in current was observed, which may arise from protein denaturation or non-specific adsorption processes.

It should be emphasized that antigen detection in this immunosensing system is primarily characterized by a decrease in current response. This phenomenon is attributed to the formation of antibody–antigen complexes on the electrode surface, which act as an insulating layer and hinder electron transfer between the redox probe and the electrode interface. Consequently, a larger current decrease corresponds to more effective antigen binding and serves as the key analytical signal for IGF-1 detection.

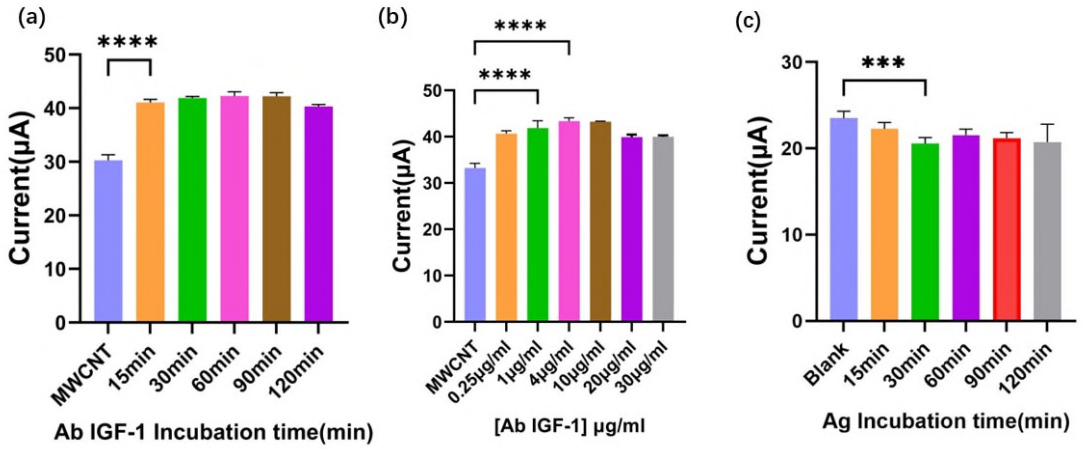


Fig. 8 (a) Optimization of anti-IGF-1 antibody incubation time (15 to 120 min) based on the

corresponding DPV current response. (b) Dependence of the DPV peak current on IGF-1 antibody concentration (0.25 to 30 μg/mL) for the MWCNTs-SPCE, referenced against a non-immobilized control. (c) Impact of IGF-1 antigen incubation time (15 to 120 min) on the DPV response after BSA blocking. Results are expressed as mean ± SD (n = 3); statistical significance (assessed by one-way ANOVA and Tukey's test) is indicated as ***p < 0.001 and ****p < 0.0001.

3. 6 Analytical performance of immunosensor

The DPV response of the proposed immunosensor across different concentrations of IGF-1, ranging from 1 to 100 μg/mL, is presented in Fig. 9(a) and (b). The DPV peak current decreased with increasing IGF-1 concentration, exhibiting a concentration-dependent behaviour. This phenomenon is attributed to the insulating effect from the abundant formation of an antibody-antigen immunocomplex at the working electrode interface. The corresponding calibration plot of DPV current response versus the logarithm of IGF-1 concentration demonstrated a strong linear correlation (R^2 = 0.9977), affirming the immunosensor's high sensitivity and reliable quantification. The selected concentration range (1–100 μg/mL) was chosen for methodological and mechanistic evaluation of the proposed immunosensor rather than direct clinical quantification. In the early stage of sensor development, relatively higher analyte concentrations are commonly employed to clearly investigate the interfacial immunoreaction behavior and the corresponding electron transfer blocking effect caused by antigen–antibody complex formation. This approach allows reliable assessment of the signal transduction mechanism and ensures accurate construction of the calibration model. Based on the 3σ/S and 10σ/S criteria [38], [39], the LOD and LOQ were calculated to be 0.95 μg/mL and 3.19 μg/mL, respectively, using a blank standard deviation (σ = 1.05 μA) and a calibration slope (S = 3.2972).

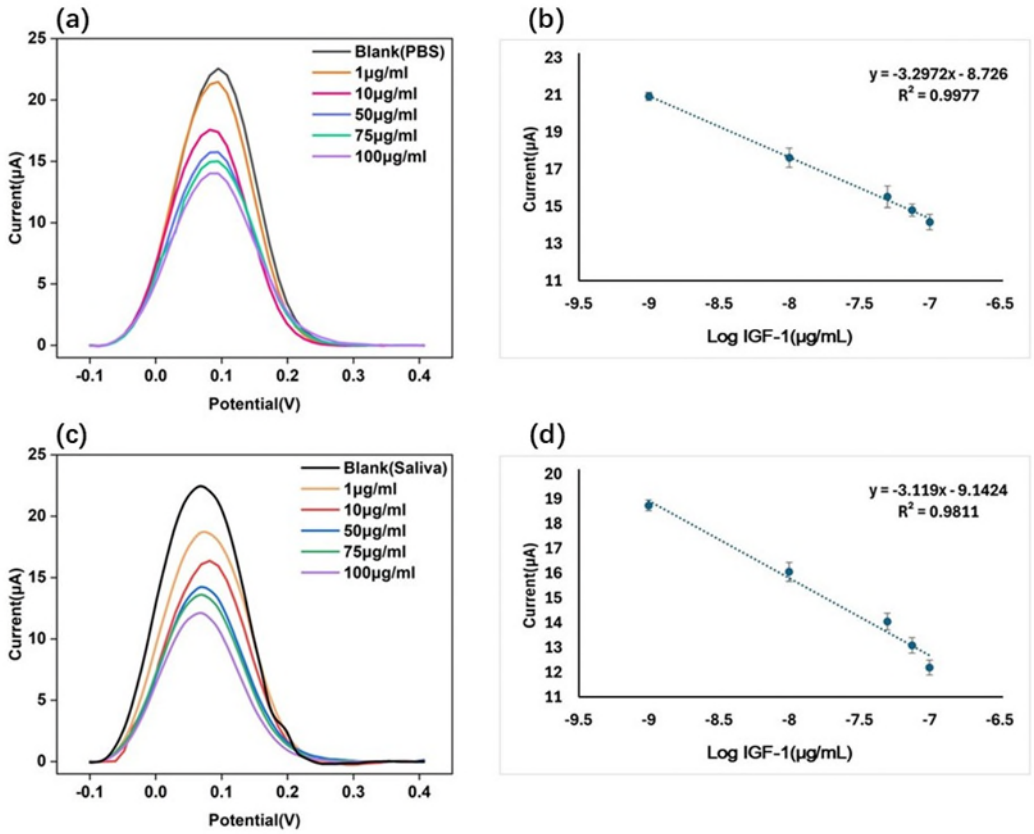


Fig. 9 DPV response and calibration curve of the immunosensor for IGF-1 detection. (a) DPV profiles obtained after incubating the immunosensor with varying IGF-1 concentrations (1–100 μg/mL in 1× PBS), using BSA as a blank control. Measurements were conducted in 0.01 M $[Fe(CN)_6]^{3-/4-}$ and 0.1 M KCl. (b) Calibration plot illustrating the relationship between DPV peak current and logarithmically scaled IGF-1 concentration, demonstrating linear behavior. (c) DPV signals of the immunosensor upon exposure to IGF-1 (1–100 μg/mL) in artificial saliva under identical conditions. (d) Corresponding calibration plot for artificial saliva matrix, illustrating a proportional correlation between peak current and log IGF-1 concentration.

The analytical performance of the immunosensor was further validated using an artificial saliva matrix. Fig. 9(c–d) demonstrates a strong linear correlation across the range of 1 to 100 μg/mL IGF-1. Accordingly, the LOD and LOQ were determined as 0.99 μg/mL and 3.3 μg/mL, respectively, using the blank standard deviation (σ = 1.03) and calibration slope (S = 3.119) for calculation. These results highlight the clinical potential of the proposed immunosensor for detecting salivary IGF-1.

Table 1 summarizes the analytical performance of the developed immunosensor in comparison with a commercially available ELISA-based IGF-1 assay kit. Although the immunosensor exhibits lower sensitivity than the commercial kit, it offers greater simplicity than traditional ELISA methods, which typically rely on sandwich immunoassays and tedious protocols [40]. Importantly, the proposed immunosensor enables non-invasive detection with minimal sample volumes (10 μL) and significantly reduces the total analysis time to 30 minutes compared to existing IGF-1 detection methods.

Table 1 Comparison of MWCNT-modified SPCE immunosensors with conventional ELISA

methods for sensitive IGF-1 assays

Immunoassay	LOD (μg/mL)	Linear Range	Sample volume (μL)	Assay time	Sample	Company
RayBio-Human IGF1 ELISA Kit	< 0.01	0.25–60 ng/mL (nonlinear)	100	4h45min	Serum, plasma, urine	RayBios
Abcam ab100545 IGF1 human ELISA Kit	< 0.01	0.123–30 ng/mL (nonlinear)	100	4h45min	Serum, plasma, urine	Abcams
Uscn E90050Hu ELISA Kit for human IGF1	< 0.01	0.094–6.0 ng/mL (nonlinear)	100	4h	Serum, plasma,	Uscn Life Science Inc.
Biorbyt Human IGF1 ELISA Kit	-	0.0625–2 ng/mL (nonlinear)	100	4h	Serum, plasma	Biorbyt Ltd.
Komabiotech Human IGF1 ELISA Kit K0332112	-	0.032–2 ng/mL (nonlinear)	100	4h30min	Serum, plasma,	Koma Biotech Inc.
Enzo IGF1 (human) ELISA Kit ADI-900–150	< 0.01	0.187–6 ng/mL (nonlinear)	100	4h	Serum, plasma	Enzos
This work	0.99	1-100 μg/mL	10	30min	Artificial Saliva	-

3. 7 Repeatability, repeatability, and stability of the immunosensor

The relative standard deviation (RSD) is a commonly used statistical measure for assessing the precision of repeated measurements. Its formula is:

$$RSD(\%) = (\frac{SD}{\overline{x}}) \times 100$$

To investigate the inter-electrode reproducibility of the prepared immunosensor, three independently prepared electrodes modified with the MWCNTs-SPCE/Anti-IGF/BSA nanocomposite were used to detect 10 μg/mL IGF-1 under identical conditions. The RSD calculated from the resulting electrochemical signals was 3.38%, indicating excellent reproducibility between different electrodes and confirming the reliability of the sensor preparation protocol.

Furthermore, to evaluate the sensor's storage stability, the sensor was stored under dry conditions at 4 °C. The electrode was removed daily and characterised using cyclic voltammetry (CV) in a solution containing 5 mM $[Fe(CN)_6]^{3-/4-}$ and 0.1 M KCl. The results showed that the peak current remained essentially unchanged over a seven-day period, although a slight decline was observed from the third day onwards, indicating that the sensor maintained reliable performance for at least three days. (Fig. 10 A and B)

Furthermore, the cycling stability was evaluated by recording the CV responses over 100 consecutive cycles (sampling only at cycles 1, 5, 10, 25, 50, 75 and 100). As shown in Fig. 10 C and D, no significant change in the current response was observed between the first and 100th cycles.

Taken together, these results indicate that the proposed immunosensor exhibits acceptable storage stability and excellent resistance to electrochemical cycling degradation.

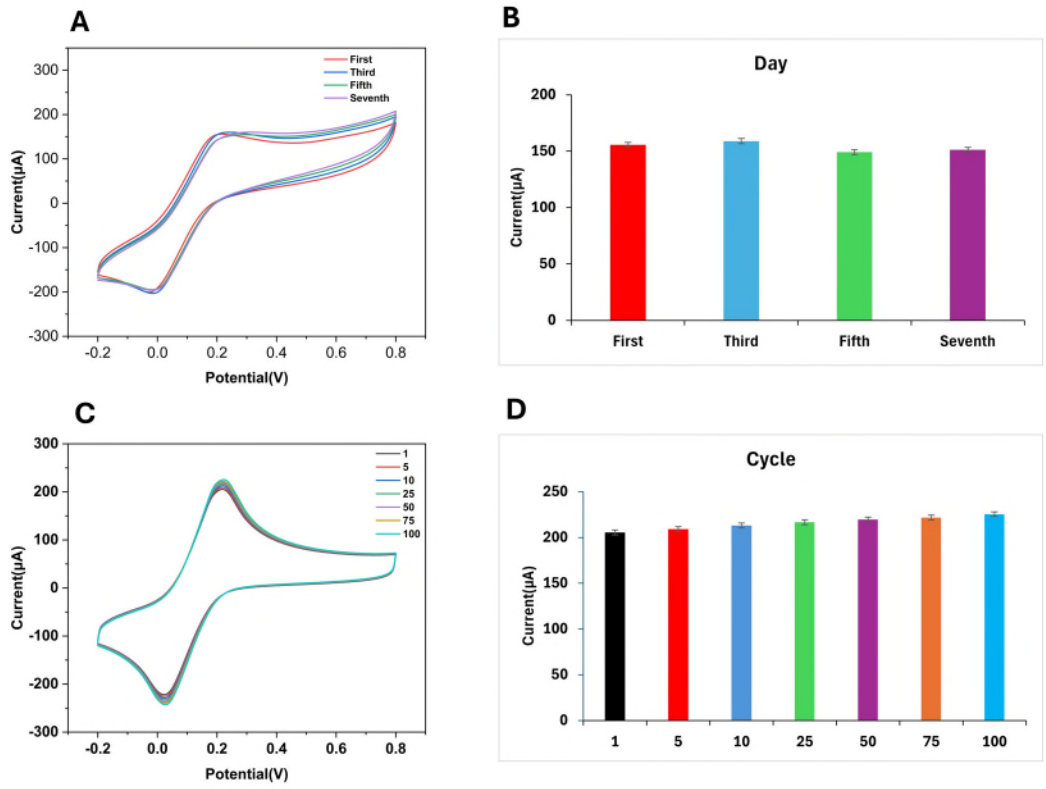


Fig. 10 (A) Corresponding peak current responses over different days, indicating the storage stability of the immunosensor under dry conditions at 4 °C. (B) Related histograms. (C) CV curves obtained over 100 consecutive cycles, used to evaluate the cycling stability.
(D) Related histograms.

4. Conclusions

In summary, this study developed an MWCNT-based electrochemical immunosensor for the quantitative detection of IGF-1 in saliva. To the best of our knowledge, this is the first non-invasive electrochemical immunosensor reported for IGF-1 detection in a saliva matrix. The proposed platform enables rapid analysis within approximately 30 min using a minimal sample volume (10 μL), offering advantages in simplicity, portability, and suitability for POC applications. It addresses key limitations of conventional IGF-1 assays, including invasive blood sampling, complex preparation steps, and reliance on centralized laboratory facilities, thereby improving accessibility and patient compliance. However, developed biosensor was evaluated using artificial saliva, and its limit of detection remains above physiological IGF-1 levels in real saliva (ng/mL range). Although its sensitivity is lower than commercial immunoassays, the platform provides a simplified and significantly faster workflow compared to ELISA-based methods. Future work will focus on improving analytical sensitivity and validating performance in real saliva samples to enable clinically relevant detection. These efforts are essential to bridge the current sensitivity gap and advance practical non-invasive IGF-1 monitoring in clinical applications.

Declaration of Competing Interest

The authors declare that they have no known competing financial interests or personal relationships that

could have appeared to influence the work reported in this paper.

Funding Declaration

This research was funded by the Impact Oriented Interdisciplinary Research Grant (IIRG) under Universiti Malaya (Grant number: IIRG002A-2022HWB) and European Union's Horizon 2020 research grant (IF005-2020 and agreement No. 872370).

REFERENCES

[1] F. Maleki, M.-R. Rashidi, H. Razmi, and M. Ghorbani, 'Label-free electrochemical immunosensor for detection of insulin-like growth factor-1 (IGF-1) using a specific monoclonal receptor on electrospun Zein-based nanofibers/rGO-modified electrode', *Talanta*, vol. 265, p. 124844, Dec. 2023, doi: 10.1016/j.talanta.2023.124844.

[2] H. Werner and Z. Laron, 'Role of the GH-IGF1 system in progression of cancer', *Mol. Cell. Endocrinol.*, vol. 518, p. 111003, Dec. 2020, doi: 10.1016/j.mce.2020.111003.

[3] A. Sookhakian, M. Zahed, H. Pakshir, and S. Ajami, 'Salivary IGF-1 and Alkaline Phosphatase-Based Modeling for Skeletal Maturity Prediction in Orthodontic Patients', *BioMed Res. Int.*, vol. 2022, no. 1, p. 2390865, Jan. 2022, doi: 10.1155/2022/2390865.

[4] J. Bailes and M. Soloviev, 'Insulin-Like Growth Factor-1 (IGF-1) and Its Monitoring in Medical Diagnostic and in Sports', *Biomolecules*, vol. 11, no. 2, p. 217, Feb. 2021, doi: 10.3390/biom11020217.

[5] A. Almalki, 'Association of Salivary IGF and IGF/IGFBP-3 Molar Ratio with Cervical Vertebral Maturation Stages from Pre-Adolescent to Post-Adolescent Transition Period—A Cross-Sectional Exploratory Study', *Int. J. Environ. Res. Public. Health*, vol. 19, no. 9, p. 5172, Apr. 2022, doi: 10.3390/ijerph19095172.

[6] M. Song, H. Bai, P. Zhang, X. Zhou, and B. Ying, 'Promising applications of human-derived saliva biomarker testing in clinical diagnostics', *Int. J. Oral Sci.*, vol. 15, no. 1, p. 2, Jan. 2023, doi: 10.1038/s41368-022-00209-w.

[7] X. Xia *et al.*, 'Sensing strategies for disease biomarkers in saliva: current status and future trends', *Coord. Chem. Rev.*, vol. 549, p. 217351, Feb. 2026, doi: 10.1016/j.ccr.2025.217351.

[8] N. V. Balashova, 'Prospects for determining insulin-like growth factor-1 in saliva', *Lab. Sluzhba*, vol. 11, no. 3, p. 24, 2022, doi: 10.17116/labs20221103124.

[9] E. Paszynska, M. Dmitrzak-Weglarz, A. Slopien, M. Tyszkiewicz-Nwafor, and A. Rajewski, 'Salivary and serum insulin-like growth factor (IGF-1) assays in anorexic patients', *World J. Biol. Psychiatry*, pp. 1–7, Apr. 2015, doi: 10.3109/15622975.2015.1023356.

[10] Y. Yasuda, 'Sex Differences in Salivary Free Insulin-Like Growth Factor-1 Levels in Elderly Outpatients', *Cureus*, Aug. 2021, doi: 10.7759/cureus.17553.

[11] A. M. Chibly, M. H. Aure, V. N. Patel, and M. P. Hoffman, 'Salivary gland function, development, and regeneration', *Physiol. Rev.*, vol. 102, no. 3, pp. 1495–1552, Jul. 2022, doi: 10.1152/physrev.00015.2021.

[12] A. Almalki *et al.*, 'Correlation between Salivary Levels of IGF-1, IGFBP-3, IGF-1/IGFBP3 Ratio with Skeletal Maturity Using Hand-Wrist Radiographs', *Int. J. Environ. Res. Public. Health*, vol. 19, no. 6, p. 3723, Mar. 2022, doi: 10.3390/ijerph19063723.

[13] A. Almalki *et al.*, 'Correlation between Salivary Levels of IGF-1, IGFBP-3, IGF-1/IGFBP3 Ratio

with Skeletal Maturity Using Hand-Wrist Radiographs', *Int. J. Environ. Res. Public. Health*, vol. 19, no. 6, p. 3723, Mar. 2022, doi: 10.3390/ijerph19063723.

[14] M. Song, H. Bai, P. Zhang, X. Zhou, and B. Ying, 'Promising applications of human-derived saliva biomarker testing in clinical diagnostics', *Int. J. Oral Sci.*, vol. 15, no. 1, p. 2, Jan. 2023, doi: 10.1038/s41368-022-00209-w.

[15] A. Almalki *et al.*, 'Correlation between Salivary Levels of IGF-1, IGFBP-3, IGF-1/IGFBP3 Ratio with Skeletal Maturity Using Hand-Wrist Radiographs', *Int. J. Environ. Res. Public. Health*, vol. 19, no. 6, p. 3723, Mar. 2022, doi: 10.3390/ijerph19063723.

[16] E. Meens Miller, N. O'Rourke, M. Jeffrey, J. Green-Johnson, and S. Dogra, 'Novel biomarkers in the saliva of healthy young males and females in a randomized crossover study on sedentary time: An exploratory analysis', *PLOS ONE*, vol. 19, no. 8, p. e0308838, Aug. 2024, doi: 10.1371/journal.pone.0308838.

[17] R. Huang, J. Shi, R. Wei, and J. Li, 'Challenges of insulin-like growth factor-1 testing', *Crit. Rev. Clin. Lab. Sci.*, vol. 61, no. 5, pp. 388–403, Jul. 2024, doi: 10.1080/10408363.2024.2306804.

[18] E. G. W. M. Lentjes, H. N. Bui, L. R. Ruhaak, I. P. Kema, K. L. M. Coene, and J. M. W. Van Den Ouweland, 'LC-MS/MS in clinical chemistry: Did it live up to its promise?', *Clin. Chim. Acta*, vol. 546, p. 117391, Jun. 2023, doi: 10.1016/j.cca.2023.117391.

[19] K. Nakane, K. Yagi, S. Yajima, S. Nomura, M. Sugimoto, and Y. Seto, 'Salivary metabolomic biomarkers for esophageal and gastric cancers by liquid chromatography–mass spectrometry', *Cancer Sci.*, vol. 115, no. 9, pp. 3089–3098, Sep. 2024, doi: 10.1111/cas.16256.

[20] F. Maleki, M.-R. Rashidi, H. Razmi, and M. Ghorbani, 'Label-free electrochemical immunosensor for detection of insulin-like growth factor-1 (IGF-1) using a specific monoclonal receptor on electrospun Zein-based nanofibers/rGO-modified electrode', *Talanta*, vol. 265, p. 124844, Dec. 2023, doi: 10.1016/j.talanta.2023.124844.

[21] V. Serafín, L. Agüí, P. Yáñez-Sedeño, and J. M. Pingarrón, 'Electrochemical immunosensor for the determination of insulin-like growth factor-1 using electrodes modified with carbon nanotubes–poly(pyrrole propionic acid) hybrids', *Biosens. Bioelectron.*, vol. 52, pp. 98–104, Feb. 2014, doi: 10.1016/j.bios.2013.08.021.

[22] F. Rossi *et al.*, 'Progress in nanoparticle-based electrochemical biosensors for hormone detection', *Nanoscale*, vol. 16, no. 39, pp. 18134–18164, 2024, doi: 10.1039/D4NR02075H.

[23] M. Liu, M. Yang, M. Wang, H. Wang, and J. Cheng, 'A Flexible Dual-Analyte Electrochemical Biosensor for Salivary Glucose and Lactate Detection', *Biosensors*, vol. 12, no. 4, p. 210, Mar. 2022, doi: 10.3390/bios12040210.

[24] S. Osaki, M. Saito, H. Nagai, and E. Tamiya, 'Surface Modification of Screen-Printed Carbon Electrode through Oxygen Plasma to Enhance Biosensor Sensitivity', *Biosensors*, vol. 14, no. 4, p. 165, Mar. 2024, doi: 10.3390/bios14040165.

[25] L. Guo *et al.*, 'Electrochemical protein biosensors for disease marker detection: progress and opportunities', *Microsyst. Nanoeng.*, vol. 10, no. 1, p. 65, May 2024, doi: 10.1038/s41378-024-00700-w.

[26] T. Yin *et al.*, 'Graphene Sensor Arrays for Rapid and Accurate Detection of Pancreatic Cancer Exosomes in Patients' Blood Plasma Samples', *ACS Nano*, vol. 17, no. 15, pp. 14619–14631, Aug. 2023, doi: 10.1021/acsnano.3c01812.

[27] A. Shabib, M. A. Maraqa, A. F. Mohammad, and F. Awwad, 'Design, fabrication, and application of electrochemical sensors for microplastic detection: a state-of-the-art review and future perspectives', *Environ. Sci. Eur.*, vol. 37, no. 1, p. 94, Jun. 2025, doi: 10.1186/s12302-025-01138-1.

[28] S. Masrat *et al.*, 'Electrochemical Ultrasensitive Sensing of Uric Acid on Non-Enzymatic Porous Cobalt Oxide Nanosheets-Based Sensor', *Biosensors*, vol. 12, no. 12, p. 1140, Dec. 2022, doi: 10.3390/bios12121140.

[29] T. Yuwen *et al.*, 'Carbon nanotubes: a powerful bridge for conductivity and flexibility in electrochemical glucose sensors', *J. Nanobiotechnology*, vol. 21, no. 1, p. 320, Sep. 2023, doi: 10.1186/s12951-023-02088-7.

[30] M. N. Norizan *et al.*, 'Carbon nanotubes: functionalisation and their application in chemical sensors', *RSC Adv.*, vol. 10, no. 71, pp. 43704–43732, 2020, doi: 10.1039/D0RA09438B.

[31] A. Kausar and I. Ahmad, 'Highpoints of carbon nanotube nanocomposite sensors—A review', *E-Prime - Adv. Electr. Eng. Electron. Energy*, vol. 7, p. 100419, Mar. 2024, doi: 10.1016/j.prime.2024.100419.

[32] M. N. Norizan *et al.*, 'Carbon nanotubes: functionalisation and their application in chemical sensors', *RSC Adv.*, vol. 10, no. 71, pp. 43704–43732, 2020, doi: 10.1039/D0RA09438B.

[33] E. M. Alosime, 'A review on surface functionalization of carbon nanotubes: methods and applications', *Discov. Nano*, vol. 18, no. 1, p. 12, Feb. 2023, doi: 10.1186/s11671-023-03789-6.

[34] N. Naeem *et al.*, 'Facile development of carbon nanotube (CNT)-based flexible thermoelectric materials for energy-harvesting applications', *RSC Adv.*, vol. 15, no. 1, pp. 569–578, 2025, doi: 10.1039/D4RA02914C.

[35] M. Patel, M. Agrawal, and A. Srivastava, 'Signal amplification strategies in electrochemical biosensors *via* antibody immobilization and nanomaterial-based transducers', *Mater. Adv.*, vol. 3, no. 24, pp. 8864–8885, 2022, doi: 10.1039/D2MA00427E.

[36] S. Tamayo-Vegas, A. Muhsan, C. Liu, M. Tarfaoui, and K. Lafdi, 'The Effect of Agglomeration on the Electrical and Mechanical Properties of Polymer Matrix Nanocomposites Reinforced with Carbon Nanotubes', *Polymers*, vol. 14, no. 9, p. 1842, Apr. 2022, doi: 10.3390/polym14091842.

[37] R. Cancelliere, E. Paialunga, A. Grattagliano, and L. Micheli, 'Label-free electrochemical immunosensors: A practical guide', *TrAC Trends Anal. Chem.*, vol. 180, p. 117949, Nov. 2024, doi: 10.1016/j.trac.2024.117949.

[38] N. I. Zakaria *et al.*, 'Thiophene structure influences plasmonic creatinine sensing through molecular interaction and surface morphology', *Sci. Rep.*, vol. 15, no. 1, p. 42967, Dec. 2025, doi: 10.1038/s41598-025-27141-3.

[39] E. Dumont *et al.*, 'Vibrational study of mycophenolic acid and its quantification with electrochemically assisted surface-enhanced Raman spectroscopy', *Sens. Actuators B Chem.*, vol. 417, p. 136126, Oct. 2024, doi: 10.1016/j.snb.2024.136126.

[40] M. Kardjadj, 'Advances in Point-of-Care Infectious Disease Diagnostics: Integration of Technologies, Validation, Artificial Intelligence, and Regulatory Oversight'.